

# Multiferroism in orientational engineered (La, Mn) co-substituted BiFeO<sub>3</sub> thin films

D. Y. Wang,<sup>1,a)</sup> N. Y. Chan,<sup>2</sup> R. K. Zheng,<sup>3</sup> C. Kong,<sup>1</sup> D. M. Lin,<sup>2</sup> J. Y. Dai,<sup>2</sup> H. L. W. Chan,<sup>2</sup> and S. Li<sup>1</sup>

<sup>1</sup>*School of Materials Science and Engineering, The University of New South Wales, Sydney, NSW 2052, Australia*

<sup>2</sup>*Department of Applied Physics and Materials Research Centre, The Hong Kong Polytechnic University, Hung Hom, Kowloon, Hong Kong, China*

<sup>3</sup>*Australian Key Center for Microscopy and Microanalysis, University of Sydney, Sydney, Australia*

(Received 29 March 2011; accepted 25 April 2011; published online 6 June 2011)

Oriental engineered (La, Mn) co-substituted BiFeO<sub>3</sub> (LMBFO) thin films were epitaxially grown on CaRuO<sub>3</sub> electroded (LaAlO<sub>3</sub>)<sub>0.3</sub>(Sr<sub>2</sub>AlTaO<sub>6</sub>)<sub>0.35</sub> (LSAT) single crystal substrates by pulsed laser deposition. The experimental results demonstrate that the crystallographic orientation is the critical dominant of the structural and multiferroic properties of LMBFO thin films. Giant remanent polarization of 65, 92, and 106  $\mu\text{C}/\text{cm}^2$  for [001], [110], [111]-oriented films, respectively, were demonstrated at room temperature. Saturated magnetization is also significantly dependent on film orientation with the highest value of 12.8 emu/cm<sup>3</sup> along [001] direction. The variation in leakage current density and ferroelectric coercivity were ascribed to the substantially difference of ferroelectric domain structures in variously oriented LMBFO thin films. © 2011 American Institute of Physics. [doi:10.1063/1.3594745]

## I. INTRODUCTION

Currently BiFeO<sub>3</sub> (BFO) is the only emerged single-phased multiferroic material with simultaneous ferroelectric and magnetic orderings at room temperature. It holds the promise for the applications of new generation memory and spintronic devices.<sup>1,2</sup> In bulk, BFO is a rhombohedrally distorted perovskite (space group R3c) presenting G-type antiferromagnetic structure with spiral spin ordering along [110] direction. Its Curie temperature  $T_c$  and Néel temperature  $T_N$  are of 1103 and 643 K, respectively. BFO materials have been extensively investigated since its large polarization was reported in strained thin films.<sup>3</sup> However, high leakage current, high coercive field and weak spontaneous magnetization in BFO thin films have become major obstacles for potentially feasible applications.

In general, the multiferroism of BFO thin films is dependent on several texture factors, including the crystallographic orientation,<sup>4–6</sup> crystallinity,<sup>7</sup> nature of the buffer layer<sup>8,9</sup> and substrates<sup>10–13</sup> etc. Additionally, many efforts have been devoted to improve the multiferroic properties of BFO utilizing cation substitution to introduce chemical pressure into the system. Both Bi- and Fe-site substitutions with a variety of cations have been attempted in BFO thin film.<sup>14–21</sup> Nevertheless, ferroelectric and magnetic behaviors of the substituted BFO thin films have great discrepancy across many research reports. The (La, Mn) co-substituting has been proposed as a promising strategy to simultaneously optimize ferroelectric and ferromagnetic properties,<sup>22–24</sup> but the co-substitution effects of La and Mn on BFO so far have only been examined in form of polycrystalline thin films with

rather scattered physical properties. In order to provide the information for revealing the intrinsic mechanism underlying the co-substitution without influences of extrinsic defects, it is desirable to investigate co-substitution effect along specific crystallographic orientation in epitaxial thin films.

High-quality BFO thin films have epitaxially grown on various single crystal substrates, including SrTiO<sub>3</sub>,<sup>3</sup> DyScO<sub>3</sub>,<sup>12</sup> and LaAlO<sub>3</sub>,<sup>25</sup> with SrRuO<sub>3</sub> as conductive buffer layers. There have very few reports, however, on BFO thin films grown on (LaAlO<sub>3</sub>)<sub>0.3</sub>(Sr<sub>2</sub>AlTaO<sub>6</sub>)<sub>0.35</sub> (LSAT) single-crystal substrates,<sup>9,26</sup> in particular adopting CaRuO<sub>3</sub> as buffer layer. As compared to a  $\sim 1.4\%$  misfit strain of commonly used SrTiO<sub>3</sub> ( $a = 3.905 \text{ \AA}$ ) with BFO ( $a = 3.96 \text{ \AA}$ ), LSAT ( $a = 3.868 \text{ \AA}$ ) offers  $\sim 2.6\%$  misfit strain, which would be more favorable for elucidating the effect of epitaxial strain on physical properties. Moreover, the orientational dependence of magnetic behaviors in BFO thin films has been rarely reported. In this work, we will take the advantages of both site engineering and strain effect imposed by the substrate to clarify crystallographic orientation dependence of multiferroic properties of (La, Mn) co-substituted BFO thin films.

## II. EXPERIMENTAL PROCEDURES

Orientation engineered (La, Mn) co-substituted BFO thin films have been epitaxially deposited on CaRuO<sub>3</sub> coated single-crystal LSAT, [001], [011], and [111] substrates, respectively, by pulsed laser deposition (PLD). The conducting perovskite oxide CaRuO<sub>3</sub> was chosen as bottom electrode material because (1) high lattice similarity with LSAT and BFO, as CaRuO<sub>3</sub> can be interpreted as a pseudocubic perovskite structure ( $a \approx 3.85 \text{ \AA}$ ) under constrained environment of epitaxial growth on a cubic substrate,<sup>27</sup> and (2) high

<sup>a)</sup>Author to whom correspondence should be addressed. Electronic mail: dy.wang@unsw.edu.au.

electrical conductivity and paramagnetic nature in whole temperature range in comparison with widely used  $\text{SrRuO}_3$ .<sup>28</sup> A 10% Bi-enriched  $(\text{Bi}_{0.90}\text{La}_{0.10})(\text{Fe}_{0.95}\text{Mn}_{0.05})\text{O}_3$  (LMBFO) target was ablated by using a KrF excimer laser (Lambda Physik COMPex 205,  $\lambda = 248$  nm) with an energy density of  $2 \text{ J/cm}^2$  and a repetition rate of 10 Hz. The distance between the target and the substrate was fixed at 5 cm, while the oxygen ambient pressure and substrate temperature was maintained at 35 Pa and  $630^\circ\text{C}$ , respectively, during laser ablation. A polycrystalline LMBFO thin film was deposited on Pt/Ti/SiO<sub>2</sub>/Si(001) under the same conditions for supplementary studies. All films were grown to a thickness of  $\sim 180$  nm to minimize film thickness effects. After deposition, the as-grown thin films were *in situ* annealed at  $630^\circ\text{C}$  under 1 atm pure oxygen for 20 min, and then gradually cooled down to room temperature.

X-ray diffraction (XRD, Bruker AXS D8 Discover, four-circle diffractometer) with Cu K $\alpha$  radiation and 4-bounce Ge(220) monochromator, and high resolution transmission electron microscopy (HRTEM, JEOL 3000FX operating at 300 kV) were used for interface analysis of thin films in atomic scale. Circular Au top electrodes with diameter of  $250 \mu\text{m}$  were prepared by rf magnetron sputtering through a shadow mask, prior to the measurement of electrical properties. Ferroelectric property measurements were conducted on TF Analyzer 2000 equipped with a FE-Module (aixACCT, Germany) by a 1 kHz triangular voltage at room temperature. Ferroelectric domain structures were imaged using a piezoresponse force microscopy (PFM, Digital Instruments, NanoScope IV). The leakage currents through the LMBFO thin film capacitors were measured using a Keithley 6517 A programmable electrometer. Magnetic properties of the thin films were studied by vibrating sample magnetometer (VSM, LakeShore 7400, Westerville, OH) at room temperature.

### III. RESULTS AND DISCUSSION

Figure 1 shows the XRD  $\theta$ - $2\theta$  spectra of [001], [110], and [111]-oriented LMBFO thin films deposited on  $\text{CaRuO}_3$ -coated LSAT, [001], [110], and [111] substrates, respectively, and a randomly oriented LMBFO thin film deposited on Pt/Ti/SiO<sub>2</sub>/Si(100) substrate. All the films grew in single-phase perovskite structure with no detectable impurity or other phases. The weak peaks for very thin  $\text{CaRuO}_3$  layer ( $\sim 40$  nm) were not resolved from the strong LSAT reflections. It is believed the good lattice match with the  $(\text{CaRuO}_3)/\text{LSAT}$  substrate promoted the growth of LMBFO phase and prevented other phases from nucleation.

The full width at half maximum (FWHM) of the x-ray rocking curves ( $\omega$  scan) for the LMBFO, [001], [011], and [111] peaks of the, [001], [011], and [111]-oriented films are  $0.73^\circ$ ,  $0.31^\circ$ , and  $0.17^\circ$ , respectively, implying that the crystallites of all three films are fairly well ordered. The in-plane texturing of the LMBFO thin films with respect to the major axes of the LSAT substrates was confirmed by the XRD  $\phi$  scan of the LMBFO (110), (010), and (100) reflections of the [001], [011], and [111]-oriented thin films, respectively. The peaks from LMBFO films coincide in position well with

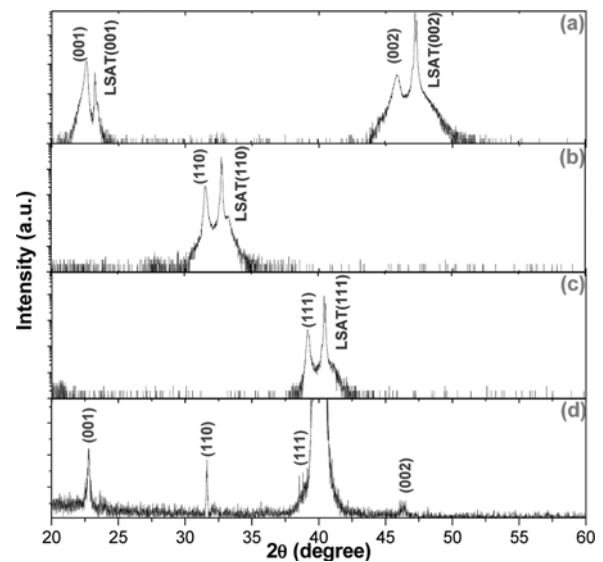


FIG. 1. (Color online) XRD  $\theta$ - $2\theta$  scans of LMBFO thin films with different orientations: (a) [001], (b) [110], (c) [111], and (d) random orientations.

those from LSAT substrates (figures not shown here), which suggests a nonlattice-rotated epitaxial growth of all the as-deposited LMBFO films. It is interesting to note that the [111]-oriented film was rhombohedral with lattice constant of  $a_r = 3.977(3) \text{ \AA}$  and  $\alpha_r = 89.31^\circ$ , which are similar as bulk material. For [110]-oriented film,  $c < a$  [ $c = 3.990(1) \text{ \AA}$ ,  $a = 4.002(6) \text{ \AA}$ ], whereas for [001]-oriented film,  $c > a$  [ $c = 3.951(7) \text{ \AA}$ ,  $a = 3.940(9) \text{ \AA}$ ], indicating the films are likely to undergo either monoclinically or tetragonally distortion. These results are in good agreement with previously reported data in pure BFO thin films.<sup>4,29</sup> The lattice distortion can be interpreted as a consequence of a compressive stress imposed by the  $\text{CaRuO}_3$  electrode, which has a smaller in-plane lattice parameter than that of LMBFO.

The structural quality of the heterostructures was further probed by electron transmission microscopy (TEM). Figures 2(a) and 2(b) show the low-magnification bright field and high resolution TEM images of LMBFO/ $\text{CaRuO}_3$ /LSAT [001] heterostructure, respectively. The film is uniform over a large area and the interfaces of LMBFO/ $\text{CaRuO}_3$  and  $\text{CaRuO}_3$ /LSAT are sharp and smooth in the magnification of observation. The high resolution image confirmed high-quality and atomically coherent interface between LMBFO thin film and the bottom electrode material  $\text{CaRuO}_3$ . Two set of diffraction patterns with the same zone axis of the films shown in Fig. 2(c) demonstrate the epitaxial relationship of LMBFO/ $\text{CaRuO}_3$  heterostructure. In addition, atomic defects including dislocation and stacking faults etc. [as arrowed in Fig. 2(b)] are also observed in the area near the interface. It is believe that the formation of atomic defects may be associated with adjustment of lattice mismatching, which is critical to ensure the growth of LMBFO epitaxial film.

The ferroelectric properties of LMBFO thin films were evaluated by a polarization-electric field ( $P$ - $E$ ) hysteresis loop as shown in Figs. 3(a)–3(d). For both epitaxial and randomly oriented films, well-defined and squarelike  $P$ - $E$  loops for a ferroelectric were observed with giant remanent polarization  $P_r$  of 65, 92, 106, and  $83 \mu\text{C/cm}^2$  for [001], [110],

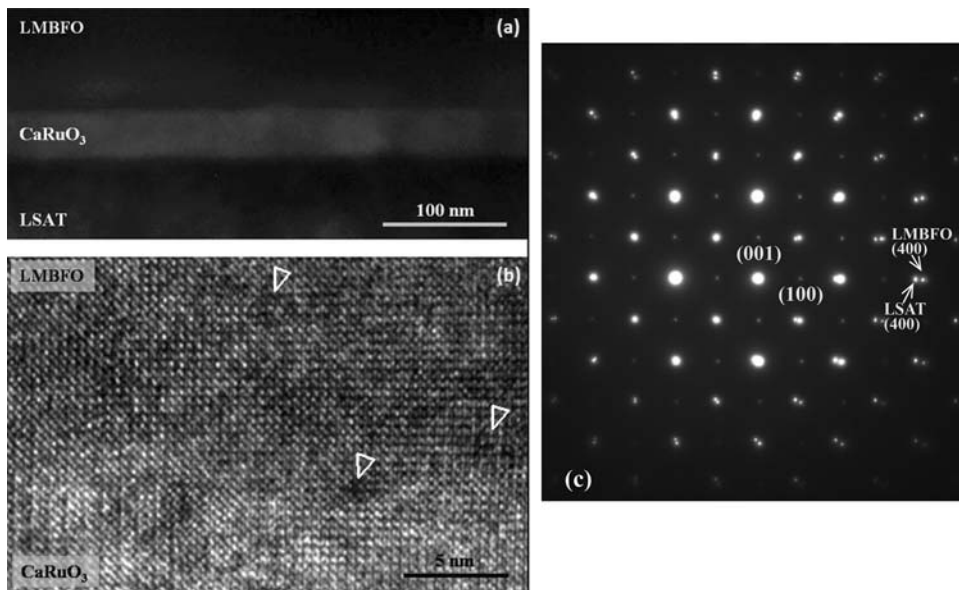


FIG. 2. (Color online) (a) Low resolution, (b) high resolution transmission electron microscopy images, and (c) selected area electron diffraction (SAED) pattern of LMBFO/CaRuO<sub>3</sub>/LSAT (001) heterostructure.

[111], and randomly oriented films, respectively. Figures 3(a)–3(c) demonstrate the good saturation characteristics of  $P_r$  and coercive field  $E_c$  of orientation engineered LMBFO thin films as a function of electric field. The  $P$ - $E$  loops illustrate two important insights. The first is that  $P_r$  is highly orientation dependent with a descending order of  $[111] > [110] > [100]$  whereas  $P_r$  for randomly oriented film is somewhere in between  $[110]$  and  $[111]$  values. It should be noted that the remanent polarization ratio of  $P_r$   $[111]: P_r$   $[110]: P_r$   $[001]$  is 1.63: 1.41: 1 and close to  $\sqrt{3} : \sqrt{2} : 1$ . This relationship is equivalent to that predicted by crystallographic considerations in rhombohedral BiFeO<sub>3</sub> crystal, where the easy axis of spontaneous polarization lies along  $[111]$  direction when Bi, Fe, and O are displaced relative to one another along this threefold axis.<sup>1,4</sup> The  $P_r$  values measured along  $[110]$  and  $[001]$  are simply projections of  $[111]$  onto these orientations. Polycrystalline LMBFO thin film grown on Pt/Ti/SiO<sub>2</sub>/Si involves great deviation from the polarization maximum direction of  $[111]$ , resulting in a weakened  $P_r$  as compared to that along  $[111]$  direction. The second finding is the  $P_r$  value of LMBFO thin films are quite comparable to that observed in BiFeO<sub>3</sub> single crystal ( $P_r \sim 60 \mu\text{C}/\text{cm}^2$  in  $[001]_c$  direction),<sup>30</sup> indicating the extremely high quality of our epitaxial LMBFO thin films. It is proposed that the enhancement in remanent polarization in comparison with pure BiFeO<sub>3</sub> thin films grown on SrRuO<sub>3</sub>/SrTiO<sub>3</sub> (001)<sup>3</sup> is mainly due to the higher degree of insulating and structural distortion caused by the dopants and substantially larger epitaxial strain imposed by CaRuO<sub>3</sub>/LSAT. It is rather difficult to obtain well established  $P$ - $E$  loops for the BFO thin films at low frequency of 1 kHz and RT, because of the high leakage current in association with various defects. High leakage current in BFO thin films is primarily due to the occurrence of a small amount of Fe<sup>2+</sup> ions, oxygen vacancies and conductive Bi<sub>2</sub>O<sub>3</sub> phase rather than the intrinsic property of BFO.<sup>31</sup> The rare-earth La substitution for volatile Bi in BFO can suppress the formation of oxygen vacancies. Mn is able to effectively suppress the

formation of Fe<sup>2+</sup> cations, as Mn can act as an acceptor to compensate the charge of Fe<sup>2+</sup> ions at the Fe site of the BFO cells. Therefore, it is quite reasonable that our LMBFO thin films possess excellent ferroelectric properties at room temperature and a relatively low leakage current as expected.

The leakage current densities of  $[111]$  and  $[001]$ -oriented films show considerably higher than that of  $[110]$ -oriented film, as shown in Fig. 4. The thin film deposited on the Pt/Ti/SiO<sub>2</sub>/Si substrate exhibits much higher leakage current than those of the films deposited on the LSAT substrates. This may be attributed to high densities of defects and oxygen vacancies, and different electrode–film interfaces in the polycrystalline film as compared with epitaxial films. Although oxygen vacancies are the most likely mobile charges and often play crucial role in the conduction of oxide ferroelectric thin films, it is believed that the magnitude of leakage currents across epitaxial LMBFO films are closely correlated with their domain wall morphology.

Figure 5 shows the ferroelectric domain structures of differently oriented LMBFO thin films imaged by piezoelectric force microscopy. It is revealed that  $[111]$  oriented film exhibits a mosaiclike domain structure, while striplike structure is the dominant domain morphology in  $[110]$ -oriented film. The  $[001]$ -oriented film shows a mixed mosaic and stripelike domain structure. Stripelike structure corresponds to arrays of 71° domain walls while the mosaiclike structure is comprised of a mixture of all possible domain wall types, particularly, large fractions of 109° domain walls and smaller fractions of 71° and 180° walls.<sup>32</sup> It has been reported that 71° domain has much lower electrostatic potential step and hence lower conductivity than 109° and 180° domains.<sup>33</sup> Consequently, it is plausible that  $[110]$ -oriented LMBFO thin film demonstrates a much lower leakage current density than films grown in other orientations.

On the other hand, as one of the most important consequences of the orientation engineering approach in our LMBFO thin films, the significant difference in ferroelectric domain structure is also responsible for the difference of

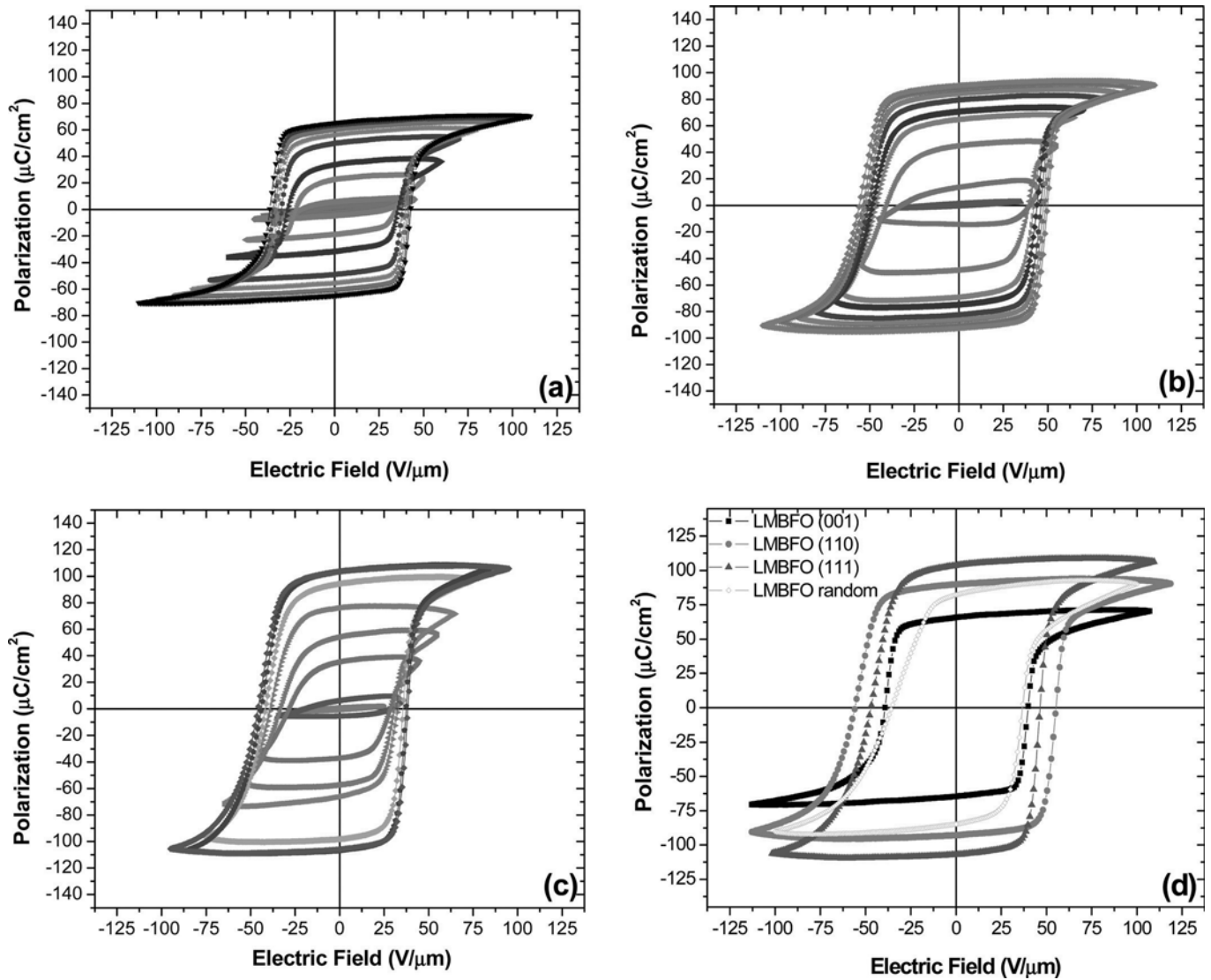


FIG. 3. (Color online)  $P$ - $E$  hysteresis loops of (a) [001], (b) [110], (c) [111]-oriented LMBFO thin films, and (d) comparison of differently oriented films.

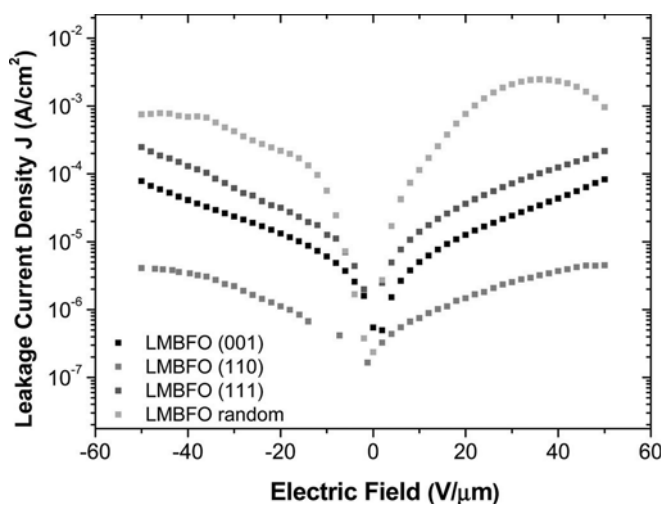


FIG. 4. (Color online) Leakage current density as a function of electric field for LMBFO thin films with various orientations.

coercive field in ferroelectric hysteresis loops. The average domain size  $d$  is determined to be  $d$  [110]  $>$   $d$  [111]  $>$   $d$  [001], indicating the highest domain wall density in [001]-oriented film. Previous research pointed out that the domain wall can be a possible scenario for low nucleation voltage in BFO thin films and a higher domain wall density leads to a lower coercive field.<sup>16</sup> This provides a good explanation to the fact that [001]-oriented film possesses the lowest coercive field, while  $E_c$  of the [110]-oriented film is the highest, as shown in Fig. 3(d).

The magnetization characteristics of all thin films were measured at a maximum magnetic field of 10 000 Oe applied either parallel or perpendicular to the substrate surface at room temperature as shown in Fig. 6. Before taking magnetic measurements, silver dag on the sides and undersides of the substrates were ground away to eliminate spurious magnetic signals from substances originating on the PLD heater block. The magnetic properties of LSAT substrate and  $\text{CaSrRuO}_3$  were measured and the results demonstrate that the

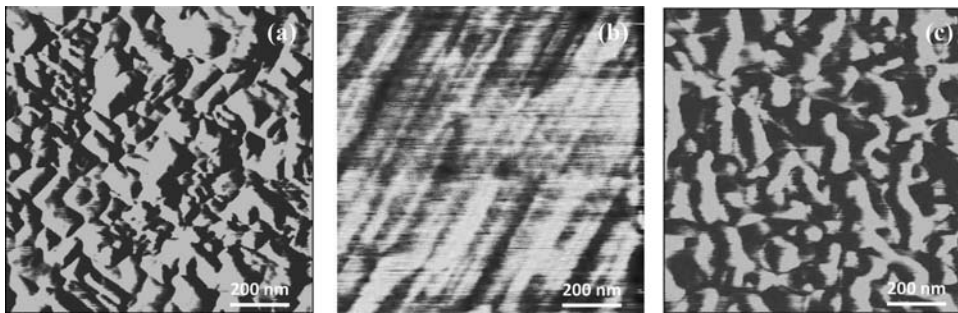


FIG. 5. (Color online) Piezoelectric force microscopy images of (a) [001], (b) [110], (c) [111]-oriented LMBFO thin films.

contribution of these components to the magnetic performance of the as-deposited LMBFO is very limited and can be ignored. Figure 6 show the magnetic hysteresis loops of the as-deposited films and it was found that the magnetic behavior is strongly orientation dependent. For instance, as shown in Fig. 6(a), the in-plane saturated magnetization  $M_s$  and coercive field  $H_c$  are 12.8 emu/cm<sup>3</sup> and 219 Oe for the [001] oriented film, 8.7 emu/cm<sup>3</sup> and 228 Oe for [110] film, 5.3 emu/cm<sup>3</sup>, and 156 Oe for [111] film, and 6.1 emu/cm<sup>3</sup> and 189 Oe for the randomly oriented films, respectively. In addition, the net magnetization is enhanced by (La, Mn) co-substitution in contrast to pure BFO [001] thin films ( $M_s \approx 7$  emu/cm<sup>3</sup>),<sup>34</sup> yielding saturation moment values in the range of 9.1–12.8 emu/cm<sup>3</sup> at a similar thickness. Bulk BFO is known to have very weak spontaneous magnetization due to its antiferromagnetic nature. Several possible considerations that are responsible for the observed magnetization in BFO thin films have been proposed:<sup>34–36</sup> The formation of parasitic phase of  $\gamma$ -Fe<sub>2</sub>O<sub>3</sub>, canting of the antiferromagnetically ordered spins through the rotation of FeO<sub>6</sub> octahedron, may suppress the inhomogeneous magnetic structure etc. We could preclude the effects of parasitic phase because our films were grown and post-annealed in sufficient oxidizing environment to restrict the formation of  $\gamma$ -Fe<sub>2</sub>O<sub>3</sub>. This is

evidenced that no reflection peaks of  $\gamma$ -Fe<sub>2</sub>O<sub>3</sub> were observed in XRD patterns. Therefore, the enhancement of magnetization is presumably a consequence of the increased spin canting angle in connection with La and Mn doping and a more homogeneous antiferromagnetic state, as the epitaxial constraint imposed by CaRuO<sub>3</sub>/LSAT is substantially sufficient to break the spiral spin ordering and thus the latent magnetization locked by the spiral is released. Neither strain nor symmetry variation would modify the type of magnetic order except for destroying the spiral modulation. In BFO thin films with absence of long-wavelength spiral spin structure, the preferred orientation of the antiferromagnetic magnetic moment should be always in the (111) plane perpendicular to the ferroelectric polarization direction, provided the film has rhombohedral symmetry.<sup>37</sup> In case of monoclinic structure, an orientation of the antiferromagnetic axis parallel to the  $[1\bar{1}0]$  direction is preferred, that is, perpendicular to the [111] axis but simultaneously parallel to the (001) plane.<sup>1</sup> Nevertheless, none of these scenarios could completely explain the observed anisotropy of magnetization in our LMBFO thin films. More work, such as x-ray magnetic linear dichroism, is needed to fully understand the spin structure and magnetic behaviors of LMBFO thin films.

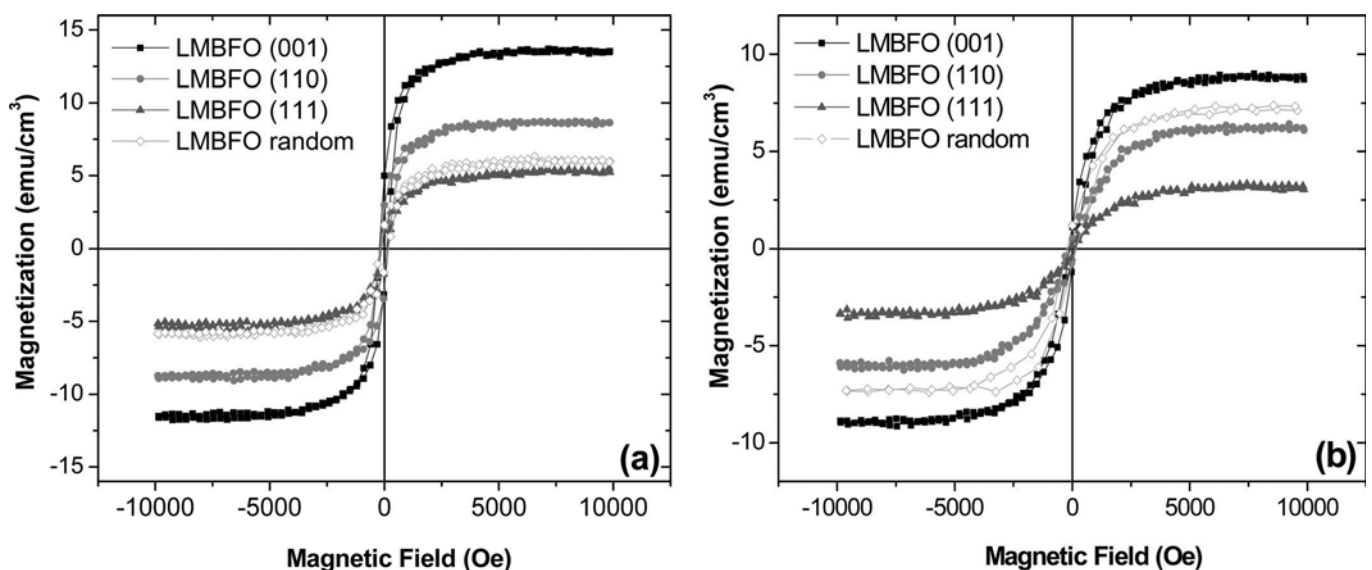


FIG. 6. (Color online) Magnetic hysteresis loops of LMBFO thin films various orientations (a) in-plane and (b) out-of-plane.

#### IV. CONCLUSIONS

In summary, this study investigated multiferroic properties of the (La, Mn) co-substituted BiFeO<sub>3</sub> thin films that were epitaxially grown on CaRuO<sub>3</sub> coated single-crystal LSAT substrates with various orientations by pulsed laser deposition. Both ferroelectric and magnetic behaviors are strongly dependent on the film orientation. The easy axis of spontaneous polarization lies close to [111] orientation with remanent polarization of 106  $\mu\text{C}/\text{cm}^2$ , whereas the highest saturated magnetization was confirmed in [001]-oriented film with  $M_s = 12.8 \text{ emu}/\text{cm}^3$  at room temperature. The morphology and structures of the ferroelectric domains are also considerably different in our LMBFO thin films. The change of ferroelectric domain structures with thin film orientation is most likely responsible for the variation in leakage current and ferroelectric coercivity.

#### ACKNOWLEDGMENTS

This work was supported by the Vice-Chancellor's post-doctoral fellowship program of the University of New South Wales (SIR50/PS16940 & IR001/PS24402) and Australian Research Council Discovery Project (Grant No. DP110104629).

- <sup>1</sup>R. Ramesh and N. A. Spaldin, *Nature Mater.* **6**, 21 (2007).
- <sup>2</sup>G. Catalan and J. F. Scott, *Adv. Mater.* **21**, 2463 (2009).
- <sup>3</sup>J. Wang, J. B. Neaton, H. Zheng, V. Nagarajan, S. B. Ogale, B. Liu, D. Viehland, V. Vaithyanathan, D. G. Schlom, U. V. Waghmare, N. A. Spaldin, K. M. Rabe, M. Wuttig, and R. Ramesh, *Science* **299**, 1719 (2003).
- <sup>4</sup>J. Li, J. Wang, M. Wutting, R. Ramesh, N. Wang, B. Buette, A. P. Pyatakov, A. K. Zvezdin, and D. Viehland, *Appl. Phys. Lett.* **84**, 5261 (2004).
- <sup>5</sup>J. G. Wu and J. Wang, *J. Appl. Phys.* **106**, 104111 (2009).
- <sup>6</sup>K. Sone, H. Naganuma, T. Miyazaki, T. Nakajima, and S. Okamura, *Jpn. J. Appl. Phys.* **49**, 09MB03 (2010).
- <sup>7</sup>J. G. Wu and J. Wang, *Acta Mater.* **58**, 1688 (2010).
- <sup>8</sup>R. Y. Zheng, C. H. Sim, and J. Wang, *J. Am. Ceram. Soc.* **91**, 3240 (2008).
- <sup>9</sup>J. G. Wu and J. Wang, *J. Am. Ceram. Soc.* **93**, 1422 (2010).
- <sup>10</sup>J. Wang, H. Zheng, Z. Ma, S. Prasertchoung, M. Wutting, R. Droopad, J. Yu, K. Eisenbeiser, and R. Ramesh, *Appl. Phys. Lett.* **85**, 2574 (2004).
- <sup>11</sup>D. S. Rana, K. Takahashi, K. R. Mavani, I. Kawayama, H. Murakami, M. Tonouchi, T. Yanagida, H. Tanaka, and T. Kawai, *Phys. Rev. B* **75**, 060405(R) (2007).
- <sup>12</sup>G. W. Pabst, L. W. Martin, Y. H. Chu, and R. Ramesh, *Appl. Phys. Lett.* **90**, 072902 (2007).
- <sup>13</sup>I. C. Infante, S. Lisenkov, B. Dupé, M. Bibes, S. Fusil, E. Jacquet, G. Geneste, S. Petit, A. Courtial, J. Juraszek, L. Bellaiche, A. Barthélémy, and B. Dkhil, *Phys. Rev. Lett.* **105**, 057601 (2010).
- <sup>14</sup>H. Naganuma, J. Miura, and S. Okamura, *Appl. Phys. Lett.* **93**, 052901 (2008).
- <sup>15</sup>S. K. Singh, H. Ishiwara, and K. Maruyama, *Appl. Phys. Lett.* **88**, 262908 (2006).
- <sup>16</sup>Y. H. Chu, Q. Zhan, C. H. Yang, M. P. Cruz, L. W. Martin, T. Zhao, P. Yu, R. Ramesh, P. T. Joseph, I. N. Lin, W. Tian, and D. G. Schlom, *Appl. Phys. Lett.* **92**, 102909 (2008).
- <sup>17</sup>G. D. Hu, X. Cheng, W. B. Wu, and C. H. Yang, *Appl. Phys. Lett.* **91**, 232909 (2007).
- <sup>18</sup>S. Fujino, M. Murakami, V. Anbusathaiah, S. H. Lim, V. Nagarajan, C. J. Fennie, M. Wutting, L. Salamanca-Riba, and I. Takeuchi, *Appl. Phys. Lett.* **92**, 202904 (2008).
- <sup>19</sup>B. F. Yu, M. Y. Li, Z. Q. Hu, L. Pei, D. Y. Guo, X. Z. Zhao, and S. X. Dong, *Appl. Phys. Lett.* **93**, 182909 (2008).
- <sup>20</sup>L. Cheng, G. Hu, B. Jiang, C. Yang, W. Wu, and S. Fan, *Appl. Phys. Exp.* **3**, 101501 (2010).
- <sup>21</sup>Z. Q. Hu, M. Y. Li, J. Liu, L. Pei, J. Wang, B. F. Yu, and X. Z. Zhao, *J. Am. Ceram. Soc.* **93**, 2743 (2010).
- <sup>22</sup>J. G. Wu and J. Wang, *J. Appl. Phys.* **106**, 054115 (2009).
- <sup>23</sup>S. Habouti, C-H. Solterbeck, and M. Es-Souni, *J. Appl. Phys.* **102**, 074107 (2007).
- <sup>24</sup>E. J. Choi, S. S. Kim, J. W. Kim, M. H. Park, H. K. Cho, W. J. Kim, S. Yi, and D. Yoo, *J. Korean Phys. Soc.* **51**, S138 (2007).
- <sup>25</sup>V. Shelke, G. Srinivasan, and A. Gupta, *Phys. Status Solidi (RRL)* **4**, 79 (2010).
- <sup>26</sup>K. Takahashi and M. Tonouchi, *Jpn. J. Appl. Phys.* **45**, L755 (2006).
- <sup>27</sup>A. Ito, H. Masumoto, and T. Goto, *J. Ceram. Soc. Jpn.* **115**, 683 (2007).
- <sup>28</sup>A. Ito, H. Masumoto, and T. Goto, *Thin Solid Films*, **517**, 5616 (2009).
- <sup>29</sup>L. Yan, H. Cao, J. Li, and D. Viehland, *Appl. Phys. Lett.* **94**, 132901 (2009).
- <sup>30</sup>D. Lebeugle, D. Colson, A. Forget, and M. Viret, *Appl. Phys. Lett.* **91**, 022907 (2007).
- <sup>31</sup>S. J. Clark and J. Robertson, *Appl. Phys. Lett.* **90**, 132903 (2007).
- <sup>32</sup>F. Zavaliche, S. -Y. Yang, T. Zhao, Y.-H. Chu, M. P. Cruz, C. B. Eom, and R. Ramesh, *Phase Trans.* **79**, 991 (2006).
- <sup>33</sup>J. Seidel, L. W. Martin, Q. He, Q. Zhan, Y. H. Chu, A. Rother, M. E. Hawkridge, P. Maksymovych, P. Yu, M. Gajek, N. Balke, S. V. Kalinin, S. Gemming, F. Wang, G. Catalan, J. F. Scott, N. A. Spaldin, J. Orenstein, and R. Ramesh, *Nature Mater.* **8**, 229 (2009).
- <sup>34</sup>W. Eerenstein, F. D. Morrison, J. Dho, M. G. Blamire, J. F. Scott, and N. D. Mathur, *Science* **307**, 1203a (2005).
- <sup>35</sup>F. Bai, J. Wang, M. Wutting, J. Li, M. Wang, A. P. Pyatakov, A. K. Zvezdin, L. E. Cross, and D. Viehland, *Appl. Phys. Lett.* **86**, 032511 (2005).
- <sup>36</sup>H. Béa, M. Bibes, S. Fusil, K. Bouzouane, E. Jacquet, K. Rode, P. Benckok, and A. Barthélémy, *Phys. Rev. B* **74**, 020101 (2006).
- <sup>37</sup>T. Zhao, A. Scholl, F. Zavaliche, K. Lee, M. Barry, A. Doran, M. P. Cruz, Y. H. Chu, C. Ederer, N. A. Spaldin, R. R. Das, D. M. Kim, S. H. Baek, C. B. Eom, and R. Ramesh, *Nature Mater.* **5**, 823 (2006).